NeuroImage 243 (2021) 118546

Contents lists available at ScienceDirect

NeuroImage

journal homepage: www.elsevier.com/locate/neuroimage

Multiscale communication in cortico-cortical networks

Vincent Bazinet[a], Reinder Vos de Wael[a], Patric Hagmann[b], Boris C. Bernhardt[a], Bratislav Misic[a,*]

[a] McConnell Brain Imaging Centre, Montréal Neurological Institute, McGill University, Montréal, Canada
[b] Department of Radiology, Lausanne University Hospital (CHUV-UNIL), Lausanne, Switzerland

ARTICLE INFO

Keywords:
Brain networks
Connectome
Structure-function
Hierarchy
Network communication

ABSTRACT

Signaling in brain networks unfolds over multiple topological scales. Areas may exchange information over local circuits, encompassing direct neighbours and areas with similar functions, or over global circuits, encompassing distant neighbours with dissimilar functions. Here we study how the organization of cortico-cortical networks mediate localized and global communication by parametrically tuning the range at which signals are transmitted on the white matter connectome. We show that brain regions vary in their preferred communication scale. By investigating the propensity for brain areas to communicate with their neighbors across multiple scales, we naturally reveal their functional diversity: unimodal regions show preference for local communication and multimodal regions show preferences for global communication. We show that these preferences manifest as region- and scale-specific structure-function coupling. Namely, the functional connectivity of unimodal regions emerges from monosynaptic communication in small-scale circuits, while the functional connectivity of transmodal regions emerges from polysynaptic communication in large-scale circuits. Altogether, the present findings reveal that communication preferences are highly heterogeneous across the cortex, shaping regional differences in structure-function coupling.

1. Introduction

The brain is a network of anatomically connected neuronal populations (Bullmore and Sporns, 2009). This complex web of connections functions as a communication network, promoting signaling between brain regions (Avena-Koenigsberger et al., 2018; Graham and Rockmore, 2011). A tendency for neuronal populations with similar functions to connect with each other gives rise to a nested hierarchy of increasingly polyfunctional neural circuits, spanning multiple topological scales (Hilgetag et al., 2000; Kaiser et al., 2010; Zhou et al., 2006).

Studies of network communication typically conceptualize signalling events as a global process, eschewing the possibility that communication takes places over multiple topological scales. Namely, areas may preferentially exchange information over small compact circuits encompassing direct neighbours and areas with similar functions, or over more extensive circuits encompassing more distant neighbours with dissimilar functions. An intuitive example is the worldwide air transportation network. The purpose of regional or domestic flights permitting transit between a country's regions is different from the purpose of international flights permitting transit between international hubs. The importance of an airport in this network will correspondingly depend on the type of flight considered. For example, Denver's and Philadelphia's airports are important for domestic flights within the United States, while airports in New York, Los Angeles or Chicago are important for international flights (Guimera et al., 2005). In other words, the topological role of a node in the network depends on the scale at which it is evaluated.

By the same token, individual brain areas may exhibit characteristic interactions and communication patterns at multiple topological scales. The modular structure of the brain (Hilgetag and Kaiser, 2004), in concert with a prominent connective core of high degree areas (van den Heuvel et al., 2012; Van Den Heuvel and Sporns, 2011), creates conditions in which information can be either segregated into local clusters of highly interconnected brain regions, or globally integrated (Zamora-López et al., 2009; 2010). For instance, an area may facilitate the integration of information among its local neighbours, but lack the capacity to globally broadcast signals across the whole brain. In other words, the functional diversity of a region – who it can communicate or interact with – should depend on scale.

A salient recent finding in connectomics is that structure-function coupling is region-specific, such that structural and functional connectivity are highly correlated in sensory cortex but poorly correlated in transmodal cortex (Baum et al., 2020; Preti and Van De Ville, 2019; Vázquez-Rodríguez et al., 2019). One prominent hypothesis is that functional connectivity in transmodal regions is less predictable because

* Corresponding author.
E-mail address: bratislav.misic@mcgill.ca (B. Misic).

https://doi.org/10.1016/j.neuroimage.2021.118546.
Received 30 April 2021; Received in revised form 27 July 2021; Accepted 31 August 2021
Available online 1 September 2021.

of the larger number of parallel and re-entrant pathways in these regions, as well as micro-architectural features that cannot be directly captured by macroscale structural connectivity (Buckner and Krienen, 2013; Vázquez-Rodríguez et al., 2019; Wang et al., 2019). An alternative hypothesis, which we directly test here, is that structural connectivity supports communication at multiple scales. Thus, there is no structure-function decoupling in transmodal cortex per se. Rather, structure-function coupling exists for all regions, but occurs in a scale-specific manner at different regions.

Here we study how communication between brain regions unfolds over multiple scales. For a given region, we systematically define local neighborhoods of increasing size. We then track how the centrality of individual brain regions varies as the sizes of the probed neighborhoods increase. We show that centrality varies across scales, and that these variations are shaped by functional diversity. We demonstrate that the unimodal-transmodal functional gradient naturally emerges from the scale preferences of individual areas, such that unimodal regions are central locally and transmodal regions are central globally. Finally, we demonstrate that structure-function coupling is scale-specific, such that the functional connectivity profiles of unimodal regions are better captured by communication within small-scale structural neighbourhoods, while the functional connectivity profiles of transmodal regions are better captured by communication within large-scale structural neighbourhoods.

2. Results

The results are organized as follows. We delineate multiscale neighborhoods by parametrically tuning the range at which signals are transmitted on the white matter connectome. We subsequently investigate the propensity for brain areas to communicate with their neighbours across multiple scales using a weighted measure of regional closeness centrality. Finally, we consider how the similarity in two areas' embedding predicts their functional connectivity. See Fig. S1 for an overview of the different measures. Data sources include (see *Materials and Methods* for detailed procedures):

- *Structural connectivity*. Structural connectomes were generated for $N = 67$ healthy participants (source: Lausanne University Hospital). Individual weighted network were reconstructed using diffusion spectrum imaging and deterministic streamline tractography.
- *Functional connectivity*. Functional connectivity was estimated in the same individuals ($N = 67$) using resting-state functional MRI (rs-fMRI).

Analyses were performed using a network parcellation of 1000 cortical nodes (Cammoun et al., 2012). They were subsequently repeated using coarser resolutions (114, 219 and 448 nodes) and an independently collected dataset (HCP; $N = 327$) (see *Materials and Methods* for more information on the *Validation* dataset).

Multiscale regional centrality

We first characterize local neighborhoods, in each structural connectome, using unbiased random walks. Specifically, we use the transition probabilities of a random walker seeded in an individual brain region to delineate its local neighborhood (see *Methods* for more details). Transition probabilities were measured for 100 time scales t, logarithmically spaced between $10^{-0.5}$ and $10^{1.5}$. Fig. 1a shows the effect of varying the scale of a random walk initiated at nodes located in the posterior cingulate (red), superior parietal (blue), transverse temporal (green) and insular (purple) cortices, with $t = 2$, $t = 5$ and $t = 10$. As t is increased, the random walks are longer and the size of the probed neighborhood becomes larger, allowing us to consider communication over more expansive portions of the network.

To investigate how the role of different brain regions varies across scales, we measure a region's closeness to other nodes in its local neighborhood. Closeness centrality is typically computed as the average of local scores measuring the inverse of the shortest path between a region of interest and each individual region in the network. Here we weight the local scores, for individual nodes, according to their proximity to the region of interest using the transition probability vector as a weight function (see *Methods*). This weight function reflects the intuition that the greater the number of electrochemical synapses a signal has to traverse, the greater the conductance time and potential attenuation of that signal (Fornito et al., 2016). When studying local interactions between proximal neuronal populations, distant neighbors become less relevant because signals cannot reach them as readily (Trusina et al., 2005). By measuring how easily a brain region can communicate with neighbors characterized across different topological scales, we obtain a multiscale measure of closeness centrality (C_{multi}).

For each time scale, we computed the C_{multi} of every brain region. Fig. 1b shows regional values of C_{multi} as t increases, averaged across subjects. To allow for comparisons between scales, C_{multi} scores are standardized relative to the distribution of scores obtained at individual scales. The centrality trajectories of four sample brain regions are highlighted, and others are shown in grey. The relative centrality of individual brain regions varies considerably with increasing scale, such that some areas are more central, and some are less central, depending on the size of their neighbourhood. Fig. 1c illustrates the centrality of every brain region, averaged across subjects, for four different topological scales. Locally, we observe clusters of highly central brain regions distributed across the whole brain; the clusters gradually evolve into larger-scale systems at more global scales.

Multiscale functional diversity

In homogeneous networks where nodes have similar topological characteristics, the local centrality of a node is expected to be similar to its global centrality. However, in heterogeneous networks, local attributes do not necessarily mirror global attributes (Estrada and Hatano, 2008). For instance, one node may have strong connectivity with a small number of nodes, while another node may have moderate but diverse connectivity with a larger number of nodes. The former is more central in a local sense, while the latter is more central in a global sense. The differential contribution of the two nodes to global communication, arising from their respective functional diversity, is reflected by their different closeness trajectories.

We illustrate this concept using an artificial network with a pre-defined modular architecture. The network of n=2000 nodes has two equally-sized communities, which are each further divided into two sub-communities (see *Methods* for the exact parameters used to construct the network). A two-dimensional embedding of the network, generated using the *ForceAtlas2* algorithm (Jacomy et al., 2014), is represented in Fig. 2a. Four nodes, labelled from i) to iv), are highlighted. To understand their contribution to global communication, it is important to not only measure the strength of their interactions with their direct neighbors (i.e. degree), but to also quantify the diversity of their connections. In a modular network, a node's connection diversity can be characterized using the participation coefficient (Guimera and Amaral, 2005). Nodes (ii) and (iv) have a large participation coefficient, meaning that they preferentially form connections with nodes outside their own communities while nodes (i) and (iii) have a small participation coefficient (Fig. 2b), meaning that they preferentially form connections with nodes within their own communities. Since node (i) preferentially forms connections with nodes inside its own community, its global centrality is smaller than its local centrality, but since node (iv) preferentially forms connections with nodes outside its own community, its global centrality is larger than its local centrality. The same reasoning applies to nodes (ii) and (iii). These variations in centrality arising from the diversity of a node's connections can be quantified using the slope of their closeness trajectories. In the case of a modular network with pre-defined communities, nodes with a positive slope have a large participation coefficient

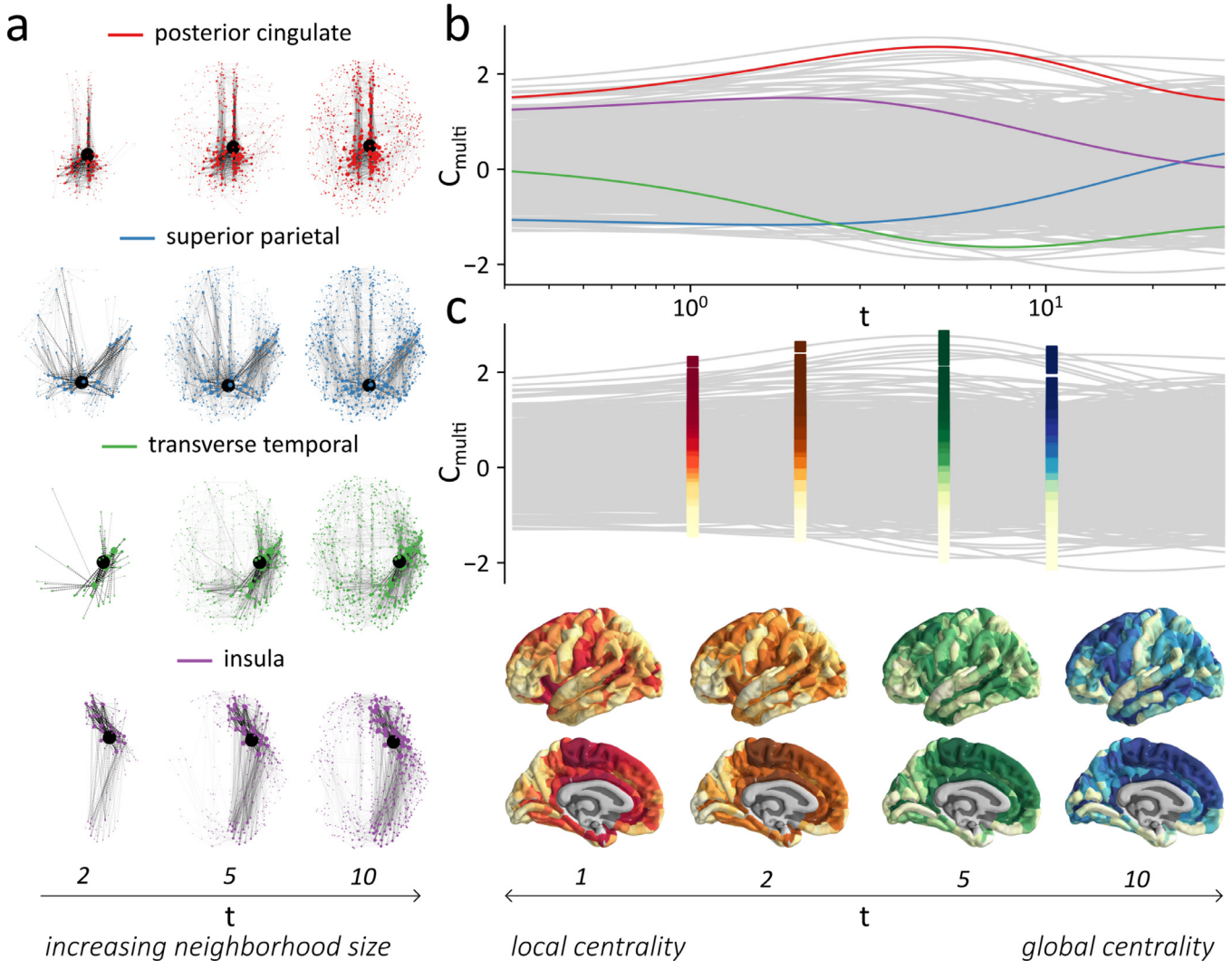

Fig. 1. Multiscale regional centrality | (a) An unbiased random-walk process can be used to delineate local neighborhoods around individual brain regions of the structural connectome. As t, the number of iterations, is increased, the topological size of the characterized neighborhoods gets larger. Random walk process can be initiated, for example, in the posterior cingulate gyrus, (red), in the superior parietal gyrus (blue), in the transverse temporal gyrus (green) or in the insula (purple), and can delineate neighborhoods of different sizes ($t = 2$; $t = 5$, $t = 10$). **(b)** The weights of a node's transition probability vector are used to compute a multiscale measure of closeness centrality (C_{multi}; see *Methods* for more details). Grey lines represent the centrality of individual brain regions, averaged across subjects, as t increases. The centrality scores are standardized for each time scale t. Highlighted in red, blue, green and purple are the centrality trajectories of the four individual brain regions shown in (a). A node's relative centrality varies largely depending on the scale of the neighborhoods. **(c)** The relative importance of a brain region in local communication processes can be evaluated by ranking C_{multi} scores within small neighborhoods ($t = 1$; left-most). Its relative importance in global processes (global centrality) can be evaluated by ranking C_{multi} scores within large neighborhoods ($t = 10$, right-most). The importance of a brain region in communication processes unfolding at intermediate scales can be similarly evaluated (e.g. $t = 2$ or $t = 5$). Darker colors indicate brain regions with large C_{multi} ranks while lighter colors indicate brain regions with low C_{multi} ranks. (For interpretation of the references to colour in this figure legend, the reader is referred to the web version of this article.)

while nodes with a negative slope have a small participation coefficient (Fig. 2d). Interestingly, slopes can be measured for any value of t, highlighting the diversity of a node's connections at the chosen scale. Slopes are correlated with local measures of diversity, such as clustering coefficient (negative correlation), when computed for small values of t, and are correlated with increasingly more global measures of diversity as t increases (Fig. 2e).

In the brain, a functionally diverse region has a topological position favoring communication across different functional modules. As such, diverse regions have properties that better support global integration (Bertolero et al., 2017; Power et al., 2013). To identify functionally diverse brain regions across scales, we computed the local slopes in the closeness centrality of individual nodes as t increases. Fig. 3a shows the C_{multi} trajectories of four nodes located in the posterior cingulate, superior parietal, transverse temporal and insular cortices (from Fig. 1a,b), colored according to their slope. Highly diverse brain regions have a positive slope (red) and less diverse brain regions have a negative slope (blue). Fig. 3b shows how the topographic distribution of these slopes on the brain varies across scales. Importantly, these slopes considers the diversity of a node's relationships across a neighborhood of arbitrary size, as opposed to a measure like participation coefficient, which only measures the diversity of its direct connections.

To demonstrate how transitions in local closeness can highlight the functional diversity of a brain region at multiple scales, we computed seven measures capturing a node's connection diversity at different topological scales. These measures are nodal strength, clustering coefficient and participation coefficients computed with respect to modular partitions of the networks into 16, 12, 9, 6 and 4 communities. For each

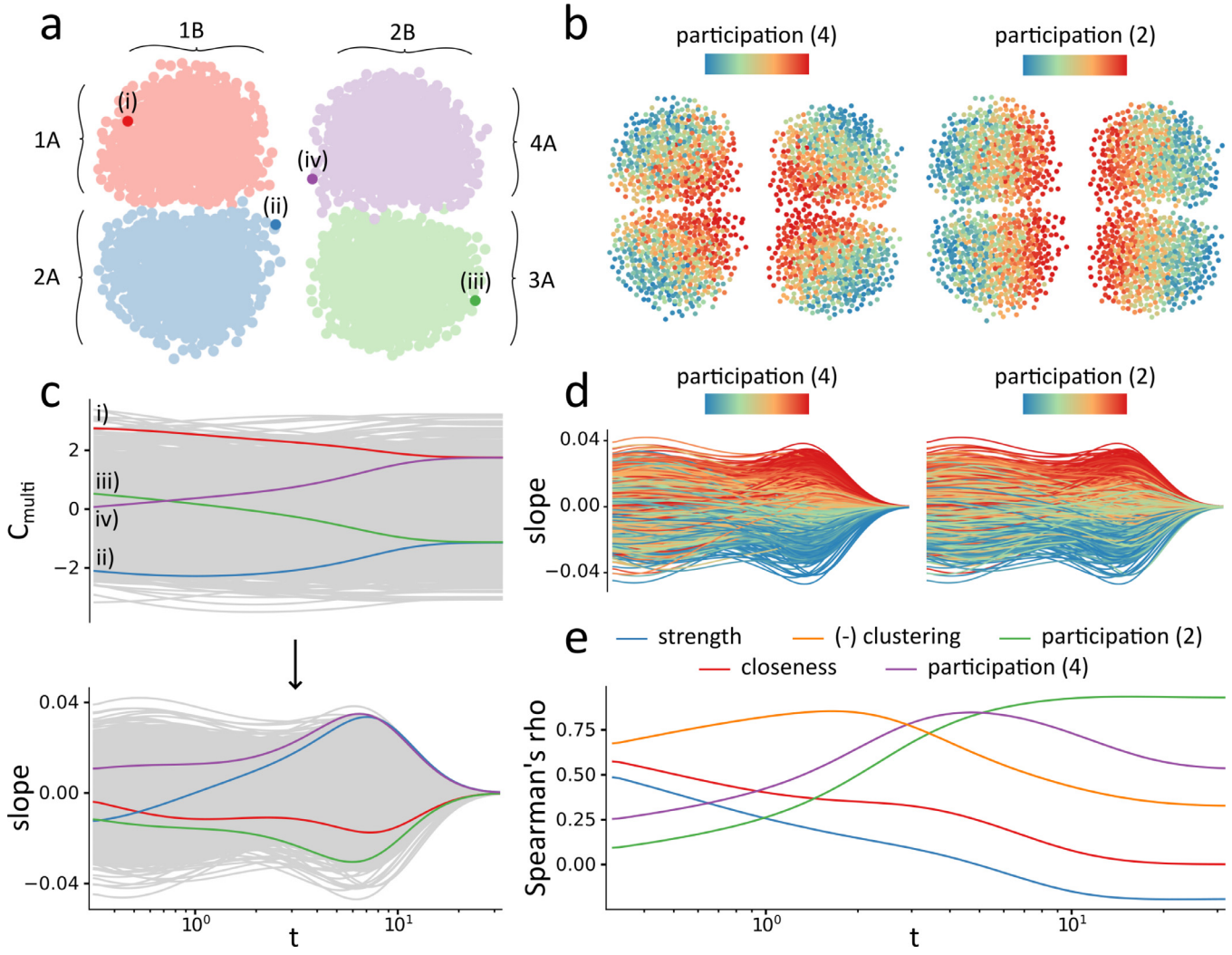

Fig. 2. Closeness trajectories in stochastic block models | (a) Two-dimensional representation of a hierarchical modular network (n=2000 nodes) generated using a stochastic-block model. Its community structure is composed of two large communities (labelled B) as well as four smaller communities (labelled A). **(b)** Participation coefficients of individual nodes for a 4-communities partition (left) and for a 2-communities partition (right). Nodes with large participation coefficients are located at the borders between the communities. **(c)** Closeness (C_{multi}) trajectories of the network's nodes, with the trajectories of the four numbered nodes in panel (a) highlighted in red, blue, green and purple. Pairs of nodes with the same global closeness centrality (red-purple; green-blue), have different trajectories (top), as anticipated by their respective locations in the low-dimensional embedding. Variations in a node's closeness can be quantified by measuring the local variations (*slope*) in their centrality (bottom). **(d)** Closeness trajectories of the network's nodes, colored according to their participation coefficients given a 4-communities parcellation (left) and a 2-communities parcellation (right). Nodes with a large participation coefficient show a positive slope and nodes with a small participation coefficient show a negative slope. **(e)** Spearman correlation between topological measures of diversity and the closeness slopes over a range of time scales. Clustering coefficient is negatively correlated with the slopes at small time scales while the two participation coefficients are strongly correlated with the slopes at larger time scales. (For interpretation of the references to colour in this figure legend, the reader is referred to the web version of this article.)

of the seven measures, we averaged the scores obtained across subjects and correlated them with the C_{multi} slopes. Fig. 3c shows the correlations between these measures and the local slopes evaluated across time scales. Measures are ordered from top to bottom according to the scale at which they are maximally correlated with the closeness slope. Local measures, such as strength and clustering coefficient, tend to be maximally correlated at lower scales ($t = 1.69$ and $t = 3.90$, respectively). Participation coefficients – indexing the diversity of inter-modular links for a given partition – tend to be correlated with local variations in closeness at greater values of t. Furthermore, as the partition resolution is gradually decreased, from 16 to 4 communities, optimal correlations are obtained at larger values of t. Altogether, these results demonstrate that variations in a node's centrality are mediated by its functional diversity. Interestingly, the present method serves to highlight functional diversity without a predefined partition, making it a complementary measure to more traditional diversity statistics (such as the participation coefficient), without the need to explicitly define or assume a hard partition.

Optimal communication scales

What is the optimal scale at which individual brain regions communicate? Fig. 4a shows the scale (t) at which the centrality of individual brain regions in the structural connectomes peaks (t_{opti}). The t_{opti} values were averaged across subjects. Cooler colors indicate regions that preferentially communicate locally while warmer colors indicate regions that preferentially communicate globally. In general, we observe preference for local communication in primary sensory regions (pericalcarine cortex, transverse temporal cortex, post-central gyrus) and in the limbic cortex; conversely, we observe preference for global communication in association cortex, including dorsolateral prefrontal cortex and superior parietal cortex.

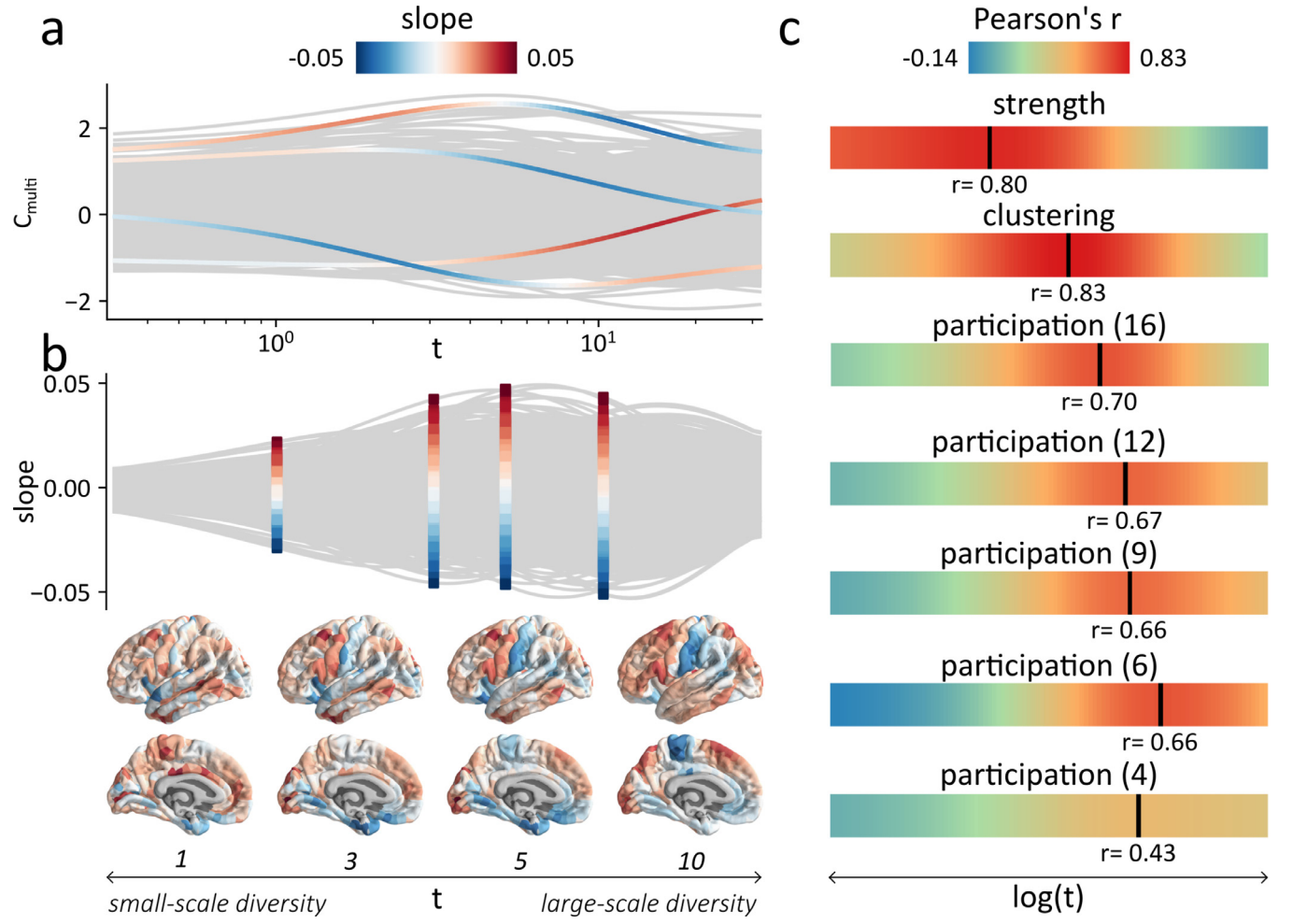

Fig. 3. Multiscale functional diversity | (a) The functional diversity of a brain region is quantified as the amplitude of the local variations in a region's closeness centrality (*slope*) as t varies. **(b)** Slopes can show different topographic distribution, for select values of t. Highly diverse brain regions have a positive slope (red) while less diverse brain regions have a negative slope (blue). **(c)** Slope scores are correlated, as t increases, with other measures of connection diversity (node degree, clustering coefficient, participation coefficients for partitions of 16, 12, 9, 6 and 4 communities). Local measures of diversity such as degree and clustering coefficient (negative) are correlated with the centrality slopes measured at intermediate scales, with peaks at $t = 1.69$ (r=0.80) for node degree and $t = 3.90$ (r=0.83) for clustering coefficient (negative). Participation coefficients, viewed as meso-scale measures of functional diversity, are also correlated with a node's local variation in centrality. The scale at which the correlation peaks highlights the size of the communities used to compute the participation coefficient, with larger values of t measuring the role of brain regions inside larger communities. (For interpretation of the references to colour in this figure legend, the reader is referred to the web version of this article.)

Fig. 4 b shows the distribution of optimal values of t for seven intrinsic functional networks (Yeo et al., 2011). These distributions are represented as heatmaps such that the nodes in the intrinsic functional networks are vertically ordered and colored based on their t_{opti} values. The mean of the distributions for the seven networks are significantly different from one another following Bonferroni correction ($p<0.001$), except for the mean t_{opti} scores of the dorsal attention and default-mode networks ($p=0.45$) and for the dorsal attention and fronto-parietal networks ($p=0.04$). These heatmaps highlight a differentiation between limbic and unimodal (somatomotor and visual) networks versus multimodal networks (default-mode, dorsal-attention and fronto-parietal networks). Fig. 4c shows, in the same way, the distribution of t_{opti} values for seven cytoarchitectonic classes defined by the von Economo atlas (von Economo and Koskinas, 1925; von Economo et al., 2008; Váša et al., 2018; Vértes et al., 2016). The means of the distributions for the primary sensory (ps) and association (ass1) classes are significantly different from the mean of the other six cytoarchitectonic classes following Bonferroni correction ($p<0.001$). These heatmaps again highlight a differentiation between sensory and association areas.

To explore the link between scale preferences and function, we extracted brain maps of probabilistic associations between functional key words and individual voxels using the Neurosynth meta-analytic engine (Yarkoni et al., 2011). We then correlated those meta-analytic maps with the centrality of individual regions across scales, and extracted the scale at which each region's centrality displays the greatest correlation with a particular term. We find that terms associated with unimodal sensory and motor functions and integration display peak correlations with the distribution of centrality values measured at local scales, and terms associated with higher-order cognitive functions display peak correlations at global scales (Fig. 4d).

We also compared the averaged C_{multi} of the seven intrinsic functional networks and cytoarchitectonic classes, as t increases, to the average C_{multi} of these intrinsic networks and classes in randomized networks with preserved degree sequences (Fig. S2). We find that the variations in C_{multi} are larger in the empirical networks than those in the randomized networks. In other words, variations in the centrality of a node are not trivially expected from their degree.

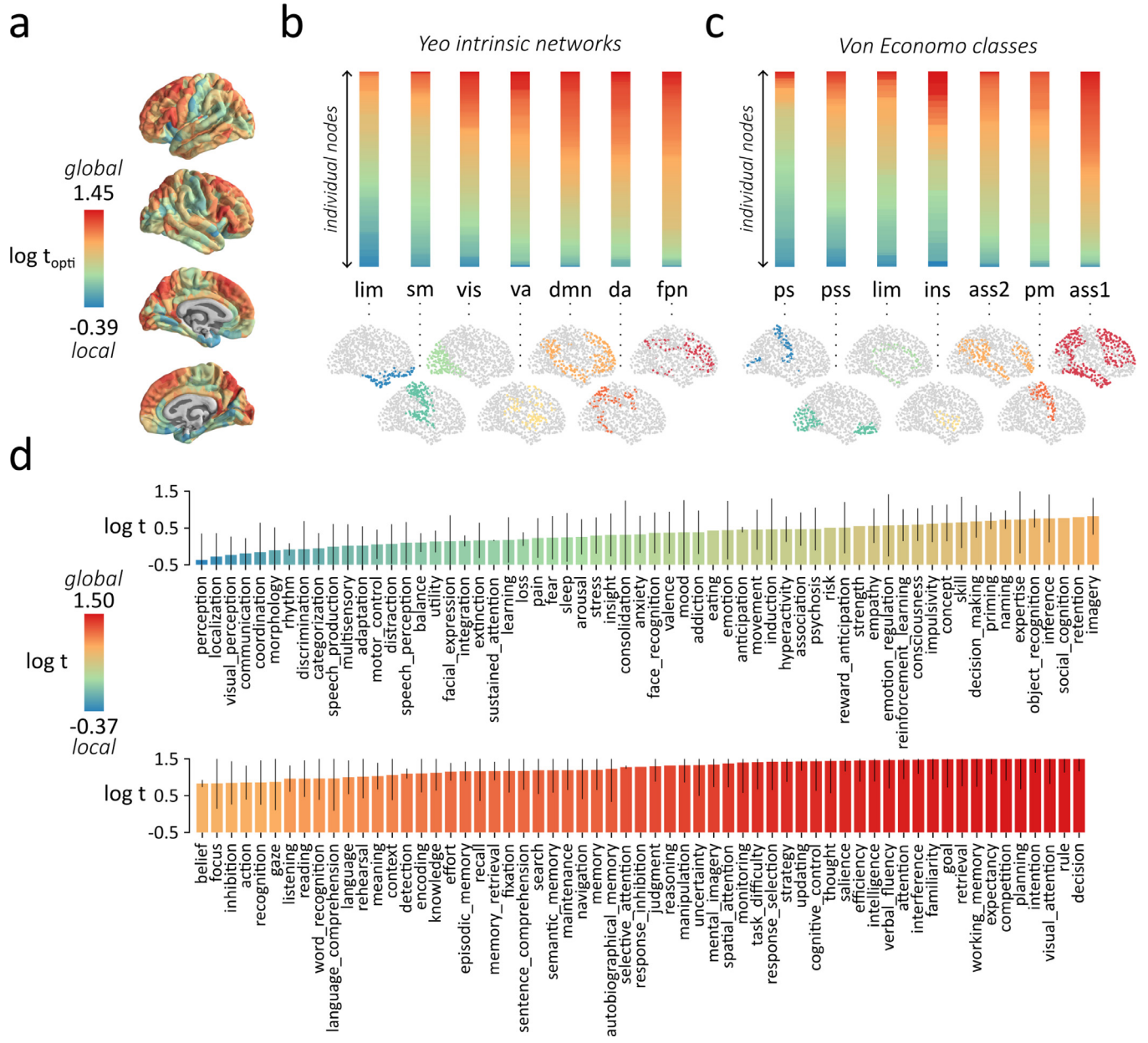

Fig. 4. Optimal communication scales | **(a)** Topographic representation of the t values at which the multiscale closeness centrality of individual brain regions of the structural connectome peaks (t_{opti}). The scores are averaged across participants. Sensory regions are optimally central for low values of t and multimodal regions are optimally central for large values of t. **(b)** Heatmaps of the distribution of optimal scale values for individual brain regions, averaged across subjects, for seven intrinsic functional networks (Yeo et al., 2011). The nodes in each heatmap are vertically ordered and colored based on their t_{opti} scores. **(c)** Heatmaps of the distribution of optimal scale values for individual brain regions, averaged across subjects, for seven cytoarchitectonic classes defined from the von Economo atlas (von Economo and Koskinas, 1925; von Economo et al., 2008; Váša et al., 2018; Vértes et al., 2016). **(d)** Scale at which the C_{multi} distributions display the greatest correlation with 123 meta-analytic maps extracted from Neurosynth (Yarkoni et al., 2011). The height and color of each bar represent the average value of t across participants while the error bars represent the standard deviation across participants. Terms associated with unimodal sensory-motor functions and integration display peak correlations with the distribution of centrality values measured at local scales (low values of t), and terms associated with higher-order cognitive functions display peak correlations at global scales (large values of t). Yeo intrinsic networks: lim = limbic network, sm = somatomotor network, vis = visual network, va = ventral attention network, dmn = default mode network, da = dorsal attention network, fpn = frontoparietal network. Von Economo classes: ps = primary sensory cortex, pss = primary/secondary sensory cortex, limbic = limbic cortex, insular = insular cortex, ass2 = association cortex 2, pm = primary motor cortex, ass1 = association cortex 1.

Multiscale structure-function coupling

We next investigate how multiscale connection patterns influence structure-function coupling. Functional connectivity between pairs of brain regions is typically computed as a correlation between the time series of their respective fMRI BOLD signals. Coherent fluctuations in neural activity are thought to arise from interactions on the underlying structural connectome (Bettinardi et al., 2017; Goñi et al., 2014; Suárez et al., 2020). A variety of pair-wise measures have been proposed to predict functional connectivity from the structural connectivity between brain regions, including structural connectivity strength, path length, search information, path transitivity (Goñi et al., 2014) and communicability (Bettinardi et al., 2017). Most of the proposed measures of structure-function coupling assume a single-scale, global relationship

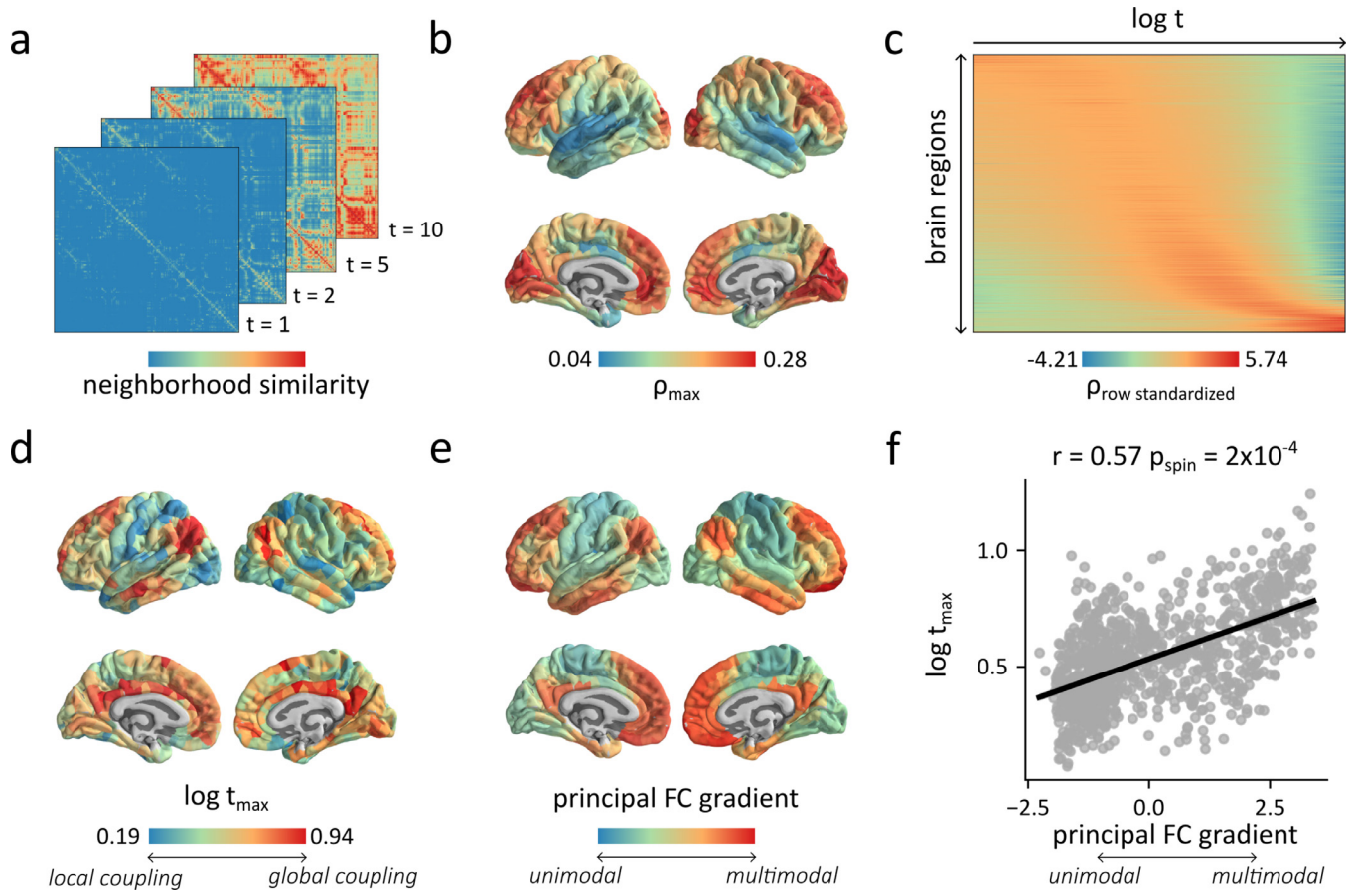

Fig. 5. Multiscale structure-function coupling | (a) Neighborhood similarity for t=1, t=2, t=5 and t=10. The neighborhood similarity between pairs of brain regions was computed as the cosine similarity between their transition probability vectors, and was computed for a range of topological scales ranging from $10^{-0.5}$ to $10^{1.5}$. **(b)** Maximal correlations between the neighborhood similarity profiles and functional connectivity profiles of individual brain regions, averaged across subjects. **(c)** Row-standardized heatmap of the correlations between the functional connectivity and neighborhood similarity profiles of individual brain regions, as t increases logarithmically. **(d)** Values of t at which the correlation between neighborhood similarity and functional connectivity profiles is maximal, for individual brain regions, averaged across subjects. **(e)** Topographic distribution of the first (principal) gradient of functional connectivity estimated using diffusion map embedding, which reflects the main organizational axis of the brain, ranging from primary sensory and motor regions to transmodal regions (Huntenburg et al., 2018; Margulies et al., 2016). **(f)** Relationship between the principal gradient of functional connectivity and log t_{max} (r=0.57; $p_{spin} = 2x10^{-4}$).

between the two (but see (Abdelnour et al., 2014; Bettinardi et al., 2017) for their use of multiscale measures).

Here we assess structure-function coupling across multiple scales. By measuring the similarity between the neighborhoods of two brain regions defined at different values of t, we ask how similar the dynamical processes unfolding around them are (Schaub et al., 2019). We hypothesize that nodes with overlapping neighborhoods (i.e. large neighborhood similarity) will display greater functional coupling than nodes that are part of different neighborhoods (Mišić et al., 2015). We hence quantified, for each structural connectome, the neighborhood similarity of pairs of brain regions by computing the pairwise cosine similarity between their transition probability vectors, for every value of t (Fig. 5a).

For every subject, we then measured the Pearson correlation between the functional connectivity and the neighborhood similarity of edges with positive functional connectivity weights. Measuring this correlation for every value of t (Fig. S3a), we find the largest correlation at $t = 2.69$ (mean = 0.22, SD = 0.03). Fig. S3b shows the distribution of individual correlation scores for each measure. The mean of the maximal correlations between functional connectivity and neighborhood similarity was significantly larger than the mean of the correlations obtained by correlating the functional connectivity matrix to the weights of the structural network's adjacency matrix (mean = 0.12, SD = 0.02; $p < 10^{-40}$), the weights of the structural network's shortest paths matrix (mean = 0.16, SD = 0.03; $p < 10^{-20}$), and the weights of the structural network's communicability matrix (mean = 0.16, SD = 0.02; $p < 10^{-25}$). The mean of these correlations was also significantly larger than the mean correlation between functional connectivity and Euclidean distance (mean = 0.20, SD = 0.03; $p = 0.00046$). These results are in accordance with previous results demonstrating that incorporating multiscale processes into structure-function coupling predictions is advantageous ((Abdelnour et al., 2014; Bettinardi et al., 2017)).

Importantly, the present framework does not assume that structure-function relationships are uniform across the brain, and instead opens the possibility that functional interactions occur at different scales for different brain regions. To investigate this possibility, we computed the Spearman correlations between the neighborhood similarity profiles and positive-valued functional connectivity profiles of individual brain regions. We averaged the correlations obtained across individual connectomes for each value of t, and identified the maximal correlation (ρ_{max}) of every brain region (Fig. 5b). We find that the optimal scale for which this regional correlation is maximal varies considerably across brain regions (Fig. 5c).

As discussed in the previous section, the optimal communication scale of brain regions varies along a unimodal-multimodal axis. We therefore hypothesize that the scale that best captures structure-function coupling for individual regions – the scale at which the correlation between neighborhood similarity and functional connectivity is maximal – similarly varies along a unimodal-multimodal axis. Fig. 5d shows the

topographic distribution of the t values at which the correlation between neighborhood similarity and functional connectivity is maximal (t_{max}). We see that the pattern indeed outlines the putative unimodal-transmodal hierarchy, such that functional connectivity profiles of unimodal regions are better captured by smaller neighbourhoods (small t), while functional connectivity in transmodal regions is better captured inside more extensive neighbourhoods. This relationship with the unimodal-transmodal hierarchy is highlighted by a significant correlation ($r = 0.57$, $p_{spin} = 2 \times 10^{-4}$) between the optimal values of t and the first (principal) gradient of functional connectivity (Figs. 5e, f). This continuous gradient, which can be estimated using diffusion map embedding, is thought to reflect the main organizational axis of the brain, ranging from primary sensory and motor regions to transmodal regions (Huntenburg et al., 2018; Margulies et al., 2016). The magnitude of the regional correlations (Fig. 5b) were not significantly correlated with the optimal scale of a brain region ($r = 0.25, p_{spin} = 0.09$) and with the first (principal) gradient of functional connectivity ($r = 0.24, p_{spin} = 0.21$), suggesting that structure-function coupling is not weaker in multimodal regions per se, but rather, that structure-function coupling is scale-specific.

We next compare the maximal correlations obtained with neighborhood similarity (ρ_{ns}) to the correlations obtained with two topological measures, namely shortest path (ρ_{sp}) and communicability (ρ_{com}), and with a geometric measure, namely Euclidean distance (ρ_{ed}). These measures have been previously used to study variations in local structure-function coupling (Vázquez-Rodríguez et al., 2019). Fig. S4a shows the relationship between the regional correlations obtained with neighborhood similarity and the correlations obtained by comparing functional connectivity to the other measures. The optimal correlations obtained with neighborhood similarity were generally larger than those obtained with the three measures. We next compute the difference between the correlation scores obtained with neighborhood similarity and the correlation scores obtained with the other three measures. We find that the largest local differences are observed in multimodal brain regions (Fig. S4b). Namely, for all three measures, neighborhood similarity was relatively better at predicting functional connectivity in multimodal brain regions. For all three measures, we found a significant correlation between the first (principal) gradient of functional connectivity and the local differences (Fig. S4c). Altogether, these results demonstrate that while other measures perform as well (or better) in the prediction of functional connectivity in sensory regions, neighborhood similarity is significantly better at predicting functional connectivity in multimodal brain regions.

Sensitivity and replication

We ultimately asked if the results are sensitive to different processing choices, if they are replicable with different parcellations and if they are replicable in an independently acquired dataset. In the present report, we delineated local topological neighborhoods using unbiased random walks. To ensure that the observed results are not dependent on our choice of this particular dynamical process, we repeated the analyses using personalized PageRank vectors (i.e. random-walks with restarts) and the normalized Laplacian matrix (i.e. diffusion process). These alternative dynamical processes also allow for multiscale investigations with a parameter that can be tuned to constrain their length (see *Methods* for more details). We also repeated the analyses using binarized networks, and to ensure that the log transformation of the streamline densities did not bias the results, we replicated all experiments using the streamline densities scaled to values between 0 and 1 as the weights of the structural connections (instead of their log-transform). To ensure that the results do not depend on parcellation resolution (Zalesky et al., 2010), we replicated all experiments with the same dataset, but parcellated into 114, 219 or 448 cortical brain regions. Finally, to ensure that the results were replicable in an independently acquired dataset, we repeated our analyses in a *Validation* dataset (HCP, N=201), which was parcellated according to a functional parcellation of 800 nodes (Schaefer et al., 2018). We obtain similar results for all sensitivity and replication experiments. The optimal communication scales are presented in Fig. S5 and Fig. S6 shows their relationship with the t_{opti} values presented in the main text. Fig. S7 shows the topographic distributions of t_{max} values, and Fig. S8 shows that those distributions are significantly correlated with the principal FC gradient. Finally, Fig. S9 shows that as the parcellations get more fine-grained, structure-function coupling must be predicted by considering dynamical processes unfolding in larger neighborhoods.

3. Discussion

In the present report, we study how inter-regional communication between brain regions occurs over multiple topological scales. By tracing the trajectory of a region's closeness in expanding neighborhoods, we identify topological attributes that mediate transitions from more localized communication to more global communication. We find that less diverse unimodal regions show preference for local communication and more diverse multimodal regions show preferences for global communication. These preferences manifest as scale-specific structure-function relationships with the functional connectivity of unimodal regions emerging from local communication in small-scale circuits and the functional connectivity of multimodal regions emerging from global communication in large-scale, poly-synaptic, circuits.

Numerous reports have found evidence of regional differences in centrality measures (Buckner et al., 2009; Gong et al., 2009; Hagmann et al., 2008; van den Heuvel and Sporns, 2013; Sporns et al., 2007; Zamora-López et al., 2010; Zuo et al., 2012). These studies were however performed at a single scale, eschewing the possibility that communication occurs across a spectrum of local, intermediate and global scales (Avena-Koenigsberger et al., 2019). In other words, they overlook the possibility that proximal populations with similar functions engage in a different mode of communication from more distant populations with dissimilar functions. Some studies, which also relied on random-walkers, investigated the multiscale community structure of brain networks (Bacik et al., 2016; Betzel et al., 2013) and showed the existence of multiple organizational scales in the brain. Our findings expand on these results as well as on previous work interested in the multiscale architecture of the brain (Betzel and Bassett, 2017) by highlighting the existence of regional heterogeneities in scale preferences. Future research could be directed towards identifying which scales are most informative (Klein and Hoel, 2020), or towards understanding how different types of biologically important dynamics, including information integration (Chang et al., 2020), synchronizability (Bassett et al., 2006), controllability (Gu et al., 2015) and complexity (Tononi et al., 1998), are constrained at multiple scales.

Heterogeneities in scale preferences naturally reveal the functional diversity of brain regions, which is typically estimated from the number of direct connections within- vs. between-modules (Guimera and Amaral, 2005; Pedersen et al., 2020). Regions with diverse connection profiles, with links to many specialized communities, are theoretically well-placed to integrate information from multiple domains (Bertolero et al., 2018; 2015; 2017; Power et al., 2013; Zamora-López et al., 2010). By considering interactions over multiple hops, we not only characterize the diversity of a node's direct connections, but also the diversity of its higher-order relationships with other regions. Moreover, our method allows for the characterization of functional diversity across a continuous range of scales, eliminating the need to partition the network into communities. This property may prove to be methodologically convenient and theoretically desirable for two reasons. First, brain networks possess prominent community structure at multiple scales, and there may not exist a single "characteristic" scale (Betzel and Bassett, 2017; Betzel et al., 2013). Second, the community structure of the brain may not be exclusively assortative (Betzel et al., 2018b; Faskowitz et al., 2018; Pavlovic et al., 2014), yet most community detection algorithms assume the presence of assortative communities (Fortunato, 2010). By track-

ing functional diversity over a range of expanding neighbourhoods, we avoid having to make assumptions about the presence, nature or scale of communities.

By identifying the optimal scale at which a brain region can communicate with neighboring regions, we find that regions participating in fewer integrative functions, such as primary visual, auditory and somatosensory cortices, optimally communicate at local scales. Conversely, polysensory regions in association or transmodal cortex optimally communicate at global scales. In other words, we show that a region's functional specialization naturally emerges from its anatomical connectivity (Mars et al., 2018; Passingham et al., 2002). We also find that neurosynth-derived functional activation maps can be ordered along this hierarchy such that terms associated with unimodal sensory and motor functions are more strongly correlated with centrality scores computed at local scales while terms associated with high-order cognitive processes are highly correlated with centrality scores computed at global scales. In other words, we find that the functional signature of a cognitive term reflects the scale of the communication processes associated with it.

Our results are naturally intertwined with the concept of segregation and integration in the brain (Sporns, 2013): local connectivity among regions with similar functions promotes specialized information processing whereas global connection patterns among regions with dissimilar functions promote integrative information processing. Future research could be directed toward understanding how scale preferences change with age. It has indeed been demonstrated that connectivity becomes less segregated with age (Betzel et al., 2014), and these changes may affect the scale at which communication processes unfold.

By tracing the trajectory of a brain region across multiple topological scales, we highlight a continuous gradient of localized versus distributed processing (Ito et al., 2020). Our results are in line with an emerging literature emphasizing large-scale gradients of cortical organization (Goulas et al., 2018; Hilgetag and Goulas, 2020; Huntenburg et al., 2018; Margulies et al., 2016; Paquola et al., 2019). Our findings offer a possible explanation for how these large-scale gradients emerge from the brain's structural embedding. Namely, at individual topological scales, areas may appear to preferentially form connections with a subset of others areas, manifesting as specific communities. As we zoom across multiple scales, however, we reveal a layered organization of interdigitated connections among areas, yielding an organizational axis of scale-specific organizational characteristics, including centrality and connection diversity. It is noteworthy that, from a geometric perspective, unimodal brain regions tend to have preferentially short-distance connections and multimodal regions have preferentially long-distance connections (Oligschläger et al., 2017; 2019; Sepulcre et al., 2010). Our results are therefore consistent with recent theories suggesting that the main role of long-distance connections is to enhance the functional diversity of a brain region (Betzel and Bassett, 2018).

This localized-distributed gradient is further highlighted by local variations in structure-function coupling. The similarity of local structural neighborhoods best predicts functional connectivity in sensory areas, suggesting that interactions among these regions unfold mainly over local, small-scale neighbourhoods. Conversely, functional connectivity in multimodal brain regions is best predicted by the topological similarity of large-scale neighborhoods, suggesting that interactions among these regions unfold mainly over more extensive, large-scale neighbourhoods. These results build upon recent reports showing that structure-function coupling is region specific (Baum et al., 2020; Demirtaş et al., 2019; Preti and Van De Ville, 2019; Suárez et al., 2020; Vázquez-Rodríguez et al., 2019; Wang et al., 2019). It has been previously hypothesized that these variations in structure-function coupling can be explained by an untethering of functional connectivity from anatomical and genetic gradients in association regions (Buckner and Krienen, 2013). Indeed, the reconfiguration of local micro-circuitry in these regions, which is marked by a greater number of parallel and reentrant pathways, may lead to greater signal variance and render structural connectivity less effective overall in predicting functional interactions. Here, we demonstrate that there is no dissociation between structural and functional properties. In fact, this observation that structure-function coupling is weaker in transmodal regions is explained by the increasing scales at which communication processes unfold. Functional connectivity in sensory regions is easier to predict from structural connectivity because it is mediated by direct communication on the structural connectome, while functional connectivity in multimodal region is harder to predict from structural connectivity because it is mediated via more indirect, polysynaptic communication pathways (Bettinardi et al., 2017).

The present findings should be interpreted with respect to several important methodological considerations. We focused on the topological organization of networks reconstructed from diffusion-weighted imaging data using computational tractometry. This approach is prone to systematic false positives and false negatives (Maier-Hein et al., 2017; Thomas et al., 2014). In addition, the connectomes generated are undirected, naturally limiting inferences about causal influence. We did, however, ensure that our results did not trivially depend on confounding factors by replicating our results using (1) different dynamical processes to generate neighborhoods, (2) different weights for our structural connectivity matrices, (3) a different parcellation resolution and (4) an independent validation dataset.

Altogether, the present findings demonstrate that exclusively considering communication at the global level might obscure functionally relevant features of brain networks. By studying regional embedding across multiple topological scales, we reveal a continuous range of communication preferences that shape structure-function relationships. In doing so, we take a step towards conceptually linking long-standing ideas in neuroscience such as integration and segregation, functional hierarchies and connection diversity.

4. Methods

Network reconstruction

All analyses were performed in two independently collected and preprocessed datasets, one collected at the Lausanne University Hospital ($N = 67$; *Discovery*) (Griffa et al., 2019) and one as part of the Human Connectome Project S900 release ($N = 327$; *Validation*) (Van Essen et al., 2013).

Discovery dataset

The $N = 67$ participants of the *Discovery* dataset (age 28.8 ± 9.1 years, 40% females) were scanned in a 3-Tesla MRI Scanner (Trio, Siemens Medical, Germany). Informed consent was obtained for all subjects (the protocol was approved by the Ethics Committee of Clinical Research of the Faculty of Biology and Medicine, University of Lausanne, Switzerland. Details regarding data acquisition, pre-processing and network reconstruction are available at (Griffa et al., 2019). Briefly, the data acquisition protocol included a magnetization-prepared rapid acquisition gradient echo (MPRAGE) sequence (1mm in-plane resolution, 1.2mm slice thickness), a diffusion spectrum imaging (DSI) sequence (128 diffusion-weighted volumes and a single b0 volume, maximum b-value 8,000 s/mm^2, 2.2 x 2.2 x 3.0 mm voxel size), and a gradient echo-planar imaging (EPI) sequence sensitive to blood-oxygen-level-dependent (BOLD) contrast (3.3 mm in-plane resolution and slice thickness with a 0.3-mm gap, TR 1,920 ms, resulting in 280 images per participant). Grey matter was parcellated into either 114, 219, 448 or 1000 equally sized parcels (Cammoun et al., 2012). The Connectome Mapper Toolkit was used for the initial signal processing (Daducci et al., 2012) while gray and white matter were segmented from the MPRAGE volume using freesurfer (Desikan et al., 2006).

Structural connectivity matrices were reconstructed for individual participants using deterministic streamline tractography on reconstructed DSI data. 32 streamline propagations were initiated per diffu-

sion direction and per white matter voxel. The weights of the edges correspond to the log-transform of the streamline density, scaled to values between 0 and 1. fMRI volumes were corrected for physiological variables (regression of white matter, cerebrospinal fluid, as well as motion), BOLD time series were subjected to a lowpass filter and motion "scrubbing" (Power et al., 2012) was performed. Functional connectivity matrices were constructed by computing the zero-lag Pearson correlation coefficient between the fMRI BOLD time series of each pairs of brain regions.

Validation dataset

The *Validation* dataset acquisition protocol included a high angular resolution diffusion imaging (HARDI) sequence and four resting state fMRI sessions. All analyses were performed in a subset of $N = 327$ unrelated participants (age 28.6 ± 3.73 years, 55% females). Out of the original 898 subjects of the S900 release of the HCP, 82 were discarded because they had missing functional or structural scans and another 353 were discarded to remove familial relationships across subjects. In the remaining 463 subjects, 184 were monozygotic twins, so we only considered one member of each pair. 20 subjects were also removed at Quality Control, and 24 were removed because they lacked DWI images. The participants were scanned in the HCP's custom Siemens 3T "Connectome Skyra" scanner. Informed consent was obtained for all subjects (the protocol was approved by the Washington University Institutional Review Board as part of the HCP). Further information regarding the acquisition protocol is available at (Van Essen et al., 2013) while more information regarding the preprocessing and the network reconstruction is available at (Park et al., 2021).

Briefly, the dMRI data was acquired with a spin-echo EPI sequence (TR=5,520 ms; TE=89.5 ms; FOV=210×180 mm ^{2}; voxel size=1.25 mm ^{3}; b-value=three different shells i.e., 1,000, 2,000, and 3,000 s/mm ^{2}; number of diffusion directions=270; and number of b0 images=18) and the rs-fMRI data was acquired using a gradient-echo EPI sequence (TR=720 ms; TE=33.1 ms; FOV=208×180 mm ^{2}; voxel size=2 mm ^{3}; number of slices=72; and number of volumes=1,200). The data was pre-processed according to the HCP minimal preprocessing pipelines (Glasser et al., 2013).

Structural connectomes were reconstructed from the dMRI data using the MRtrix3 package (Tournier et al., 2019). Fiber orientation distributions were generated using a multi-shell multi-tissue constrained spherical deconvolution algorithm (Dhollander et al., 2016; Jeurissen et al., 2014). The initial tractogram was generated with 40 million streamlines, with a maximum tract length of 250 and a fractional anisotropy cutoff of 0.06. Spherical-deconvolution informed filtering of tractograms (SIFT2) was used to reconstruct whole brain streamlines weighted by cross-section multipliers (Smith et al., 2015). To ensure that our results were not confounded by the parcellation scheme or resolution, grey matter was parcellated with a different parcellation. This time, grey matter was parcellated into 800 cortical regions according to the Schaefer functional atlas (Schaefer et al., 2018). Functional connectivity matrices were constructed for individual subjects by computing the zero-lag Pearson correlation coefficient between the fMRI BOLD time series of each pairs of brain regions. The functional weights of the four resting-state sessions were then averaged for each individuals.

Yeo intrinsic networks and von Economo classes

To facilitate our analyses, nodes of the brain networks were stratified according to their membership to seven intrinsic functional networks and seven cytoarchitectonic classes. The seven intrinsic functional networks were identified by applying a clustering technique on resting-state fMRI data from 1000 subjects. More details can be found in (Yeo et al., 2011). The seven resting-states parcellation, in the FreeSurfer fsaverage5 surface space, was first downloaded from https://github.com/ThomasYeoLab/CBIG/. We then attributed to each parcel of the 1000 nodes Cammoun parcellation the most common intrinsic network assignments of its vertices. The seven cytoarchitectonic classes consist in an extended version of the classical von Economo atlas (von Economo and Koskinas, 1925; von Economo et al., 2008). The class of each parcel was manually assigned based on visual comparison with the von Economo and Koskinas's parcellation and anatomical landmarks (Váša et al., 2018; Vértes et al., 2016).

Multiscale topological neighborhoods

Local neighborhoods were characterized by modelling dynamical process initiated from individual nodes in the networks. By controlling the length of these processes, we controlled the topological size of the delineated neighborhoods. Our main results relied on unbiased random-walks. We further replicated our results using random walks with restarts and a heat-diffusion process.

Unbiased random-walks

Given a weighted adjacency matrix $\mathbf{A}$ where A_{ij} corresponds to the weight of the edge connecting nodes i and j, the probability that a walker at node i transitions to node j in a single iteration is given by $\frac{A_{ij}}{d_i}$, where d_i is the strength of node i and corresponds to the sum of the weights of the edges leaving the node. For the experiments presented in the main text, the weights of the adjacency matrix were chosen as the log-transform of the streamline densities, scaled to values between 0 and 1. As such, transition probabilities are larger between regions connected by denser streamlines. We also replicated our experiments using the streamline densities scaled to values between 0 and 1 as weights (no log transform), and using the binary connectome. The overall transition probabilities of a network can be represented in a transition matrix $\mathbf{P}$ such that:

$$\mathbf{P} = \mathbf{D}^{-1}\mathbf{A}, \tag{1}$$

where $\mathbf{D}$ is the diagonal matrix with the value D_{ii} corresponding to the strength of node i. Given an initial distribution of random walkers $\mathbf{p}(0)$, it is possible to compute the distribution of these random walkers at a discrete time t, $\mathbf{p}(t)$:

$$\mathbf{p}(t) = \mathbf{p}(0)\mathbf{P}^t. \tag{2}$$

The vector $\mathbf{p}(t)$ indicates the proportion of walkers located at any other node at time t. We initiate this random walk process on a single node i by setting the initial distribution $\mathbf{p}(0)$ to be equal to 0 everywhere, and be equal to 1 in position i. This initial vector can be written as $\mathbf{e}_i$. The transition probability vector at time t, given that the random walk process was started on node i can then be written as:

$$\mathbf{p}(t|i) = \mathbf{e}_i\mathbf{P}^t. \tag{3}$$

The discrete-time random walk process defined above can be "continuized" by considering the interval of time between two moves as an exponential random variable with $\lambda = 1$ (Masuda et al., 2017). The transition probability vector, for a random walk process initiated on node i, is then given by:

$$\mathbf{p}(t|i) = \mathbf{e}_i(e^{-t\mathbf{L}_{rw}}), \tag{4}$$

where $\mathbf{L}_{rw} = \mathbf{I} - \mathbf{P}$ is the graph random-walk normalized Laplacian.

By initiating a random-walk process from a single node, we can measure the topological proximity between this node and the other nodes in the network. By increasing the value of t, we increase the length of the random-walks, and consequently measure the topological proximity of nodes in larger neighborhoods. We measured the transition probabilities for 100 time scales t, logarithmically spaced between $10^{-0.5}$ and $10^{1.5}$.

Random-walks with restarts

A variant of this equation consists in adding to this random-walk process an additional probability that the random walker randomly teleports itself back to the seed node. Random walks with teleportation are

the basis for the PageRank algorithm (Brin and Page, 1998) and ensure that random walks on directed networks do not get trapped in absorbing states. The equation, given that the random walk process is initiated on a single node i, is defined as follows:

$$\mathbf{p}(t|\alpha, i) = (\alpha)\mathbf{e}_i\mathbf{P}^t + (1-\alpha)\mathbf{e}_i, \tag{5}$$

where α corresponds to the damping factor. By varying the damping factor, we can decrease the probability of restart of the random walks and therefore increase their length. More specifically, the probability that a random-walks is of length l ($Prob[L = l]$) is geometrically related to the value of the parameter α:

$$Prob_\alpha[L = l] = (1-\alpha)\alpha^l. \tag{6}$$

Ultimately, the stationary distribution of this Markov chain, which can be computed using the power iteration method, indicate the probability that random walkers of a certain length, starting from a single source node, reach other nodes in the network. We computed the stationary distribution, also known as the personalized PageRank, for 99 values of α, linearly spaced between 0.01 and 0.99.

Diffusion

An alternative method to dynamically measure the topological proximity of brain regions in a network consists in modelling a heat-diffusion process on the network. More specifically, the Laplacian matrix (**L**) of the network is used to compute the distribution of some material at time t, given that the process was initiated at node i:

$$\mathbf{p}(t|i) = \mathbf{e}_i(e^{-t\mathbf{L}})_{ij}, \tag{7}$$

where

$$\mathbf{L} = \mathbf{I} - \mathbf{D}^{-1/2}\mathbf{A}\mathbf{D}^{-1/2}. \tag{8}$$

Again, by varying the value of t, we can vary the size of the neighborhoods on which the diffusion process unfolds, and therefore measure the topological proximity of nodes in the network given dynamical processes unfolding at increasingly large scales. We measured the transition probabilities for 100 time scales t, logarithmically spaced between $10^{-0.5}$ and $10^{1.5}$.

Multiscale closeness centrality

Measures of network centrality often consider a node's relationship with all of the other nodes. For instance, the closeness centrality of a node in a network can be measured by computing the inverse of its averaged topological distance to the other nodes in the network:

$$C(i) = \frac{n-1}{\sum_j \phi_{ij}}, \tag{9}$$

where n corresponds to the number of nodes in the network parcellation and ϕ_{ij} corresponds to the weighted shortest path between nodes i and j.

To capture the centrality of a node at different scales, we propose a new measure. This measure consists in computing the multiscale closeness centrality of a node as a weighted average using the probability vector **p** as a weight function prioritizing the node's relationships with nodes that are topologically close over nodes that are topologically remote. Specifically, given a scale-dependent weight vector $\mathbf{p}(t|i)$, the multiscale closeness centrality of a node i for the specified scale t is defined as:

$$C_{\text{multi}}(i|t) = \frac{1}{\sum_j p_j(t|i)\phi_{ij}}. \tag{10}$$

The topological distance between a pair of connected nodes i and j was measured as the inverse of the connection weight between the two nodes, and the topological shortest paths between pairs of nodes were subsequently retrieved using the Dijkstra's algorithm. The code to compute this multiscale measure of closeness centrality is available in the project's github repository (https://github.com/netneurolab/bazinet_multiscale)

Multiscale functional diversity

Analogous to techniques like Infomap (Rosvall and Bergstrom, 2008), we make use of the fact that highly interconnected regions trap random-walkers to capture the functional diversity of individual nodes in a network. As walkers centered on a node diffuse over larger neighborhoods, they start to encounter distinct functional clusters. These transitions in the local architecture of the network give rise to variations in centrality. A node that preferentially forms connections with functionally similar nodes will have a decreasing trajectory while a node that preferentially forms connections with dissimilar nodes will have an increasing trajectory. The slope of C_{multi} reflects how the importance of a node diminishes or increases across scales. The slope in the centrality of a node i, for a scale t is computed as the central difference approximation:

$$slope(i|t) = \frac{C_{\text{multi}}(i|t+h) - C_{\text{multi}}(i|t-h)}{2h}, \tag{11}$$

where h is the spacing between each value of t.

Probabilistic activation maps

Using the Neurosynth meta-analytic engine (Yarkoni et al., 2011) we extracted brain maps of probabilistic associations between functional key words and individual voxels, synthesized from results from more than 15,000 published fMRI studies. The probabilistic measures, which consist in the probability that a given term is reported in a study and that there is activation observed in a given voxel, can be interpreted as a quantitative representation of how regional fluctuations in activity are related to psychological processes. We analyzed the functional maps associated to 123 cognitive and behavioural terms from the Cognitive Atlas ((Poldrack et al., 2011), ranging from umbrella terms ("attention", "emotion") to specific cognitive processes ("visual attention", "episodic memory"), behaviours ("eating", "sleep"), and emotional states ("fear", "anxiety").

Clustering coefficient

The clustering coefficient of a node corresponds to the number of triangles attached to it, normalized by the maximum number of possible triangles that could be attached to the node (Watts and Strogatz, 1998):

$$C(i) = \frac{2t_i}{k_i(k_i-1)}, \tag{12}$$

where k_i is the degree of node i and t_i is the number of triangles attached to node i. A weighted version of the clustering coefficient, which can be viewed as a measure of the average "intensity" of triangles around a node, can also be expressed as follows (Onnela et al., 2005):

$$C_w(i) = \frac{2}{k_i(k_i-1)}\sum_{jk}(\tilde{w}_{ij}\tilde{w}_{jk}\tilde{w}_{ki})^{\frac{1}{3}}, \tag{13}$$

where $\tilde{w_{jk}}$ is the weight of the connection between nodes j and k, divided by the largest weight in the network. The clustering coefficients were computed using the Brain Connectivity Toolbox (https://github.com/aestrivex/bctpy) (Rubinov and Sporns, 2010).

Community detection

Communities are groups of nodes with dense connectivity among each other. The Louvain method was used to identify a community assignment or partition that maximizes the quality function Q (Blondel et al., 2008):

$$Q = \frac{1}{2m}\sum_{i,j}\left[A_{ij} - \gamma\frac{s_i s_j}{2m}\right]\delta(c_i.c_j), \tag{14}$$

where A_{ij} is the weight of connection between nodes i and j, s_i and s_j are the directed strengths of i and j, m is a normalizing constant, c_i

is the community assignment of node i and the Kronecker δ-function $\delta(u, v)$ is defined as 1 if $u = v$ and 0 otherwise. The resolution parameter γ scales the importance of the null model and effectively controls the size of the detected communities: larger communities are more likely to be detected when $\gamma < 1$ and smaller communities (with fewer nodes in each community) are more likely to be detected when $\gamma > 1$.

To detect stable community assignments for our structural connectomes, we first constructed a consensus network from the individual connectomes. This network was generated such that the mean density and edge length distribution observed across individual participants was preserved (Betzel et al., 2018a; Mišić et al., 2018; 2015). The edges were weighted as the average weight across individual networks for which these edges existed. Using this consensus network, we initiated the algorithm 100 times at each value of the resolution parameter and consensus clustering was used to identify the most representative partitions (Lancichinetti and Fortunato, 2012). This procedure was repeated for a range of 100 resolutions between $\gamma = 0.25$ and $\gamma = 7.5$. We then quantified the similarity between pairs of consensus partitions using the z score of the Rand index (Traud et al., 2011). We next identified five values of γ at which the generated partitions showed high mutual similarity and persisted through stretches of γ values. This procedure yielded partitions of 4, 6, 9, 12 and 16 communities (corresponding to γ=0.54, 1.08, 2.06, 2.85, 7.16). The whole procedure was implemented using code available in the netneurotools python toolbox (https://github.com/netneurolab/netneurotools).

Participation coefficient

Given a partition, we quantify the diversity of a node's connections to multiple communities using the *participation coefficient* (Guimera and Amaral, 2005). The participation coefficient is defined as

$$pc_i = 1 - \sum_{c \in C} \left[\frac{s_i(c)}{s_i} \right]^2, \tag{15}$$

where s_i is the total strength of node i, $s_i(c)$ is the strength of i in community c and the sum is over the set of all communities C. Nodes with a low participation coefficient are mainly connected with nodes in a single community, while nodes with a high participation coefficient have a diverse connection profile, with connections to multiple communities. The participation coefficients were computed using the Brain Connectivity Toolbox (https://github.com/aestrivex/bctpy) (Rubinov and Sporns, 2010).

Autocorrelation-preserving permutations

To assess the significance between the principal functional connectivity gradient and t_{max}, we relied on autocorrelation-preserving permutations and generated null distributions that preserve the spatial autocorrelation of the original brain map. By preserving this autocorrelation, we ensure that the null distributions do not violate the assumption of exchangeability and that permutation tests will not generate inflated p-values (Alexander-Bloch et al., 2018; Markello and Misic, 2021). To generate autocorrelation-preserving permutations, we first created a surface-based representation of the Cammoun atlas on the FreeSurfer fsaverage surface using the Connectome Mapper toolkit (https://github.com/LTS5/cmp, (Daducci et al., 2012)). We identified the vertices closest to the center-of-mass of each parcel and used the spherical projection of the fsaverage surface to define spherical coordinates for each parcel. We then applied randomly-sampled rotations to the spherical atlas and reassigned each parcel to the closest parcel following this rotation. Each rotation was applied to one hemisphere and then mirrored to the other hemisphere. This process was repeated 10,000 times using code available in the netneurotools python toolbox (https://github.com/netneurolab/netneurotools). The empirical distributions were then compared to these spatially-autocorrelated nulls and two-sided p-values (p_{spin}) were computed.

Neighborhood similarity

The pairwise neighborhood similarity of nodes in the network, for a particular scale t can be represented in a matrix $\mathbf{S}(t)$, where $S_{ij}(t)$ corresponds to the cosine similarity between the transition probability vectors of nodes i and j, for the scale t:

$$S_{ij}(t) = 1 - \frac{\mathbf{p}(t|i)\mathbf{p}(t|j)}{\|\mathbf{p}(t|i)\mathbf{p}(t|j)\|}. \tag{16}$$

The code to compute neighborhood similarity is available in the project's github repository (https://github.com/netneurolab/bazinet_multiscale).

Communicability

For a binary adjacency matrix $\mathbf{A}$, communicability is defined as

$$C_{ij} = \sum_{n=0}^{\infty} \frac{[\mathbf{A}^n]_{ij}}{n!} = [e^{\mathbf{A}}]_{ij}, \tag{17}$$

with walks of length n normalized by $n!$, ensuring that shorter, more direct walks contribute more than longer walks (Estrada and Hatano, 2008). For a weighted adjacency matrix, this definition can be extended as

$$C_{ij} = (exp(\mathbf{D}^{-1/2}\mathbf{A}\mathbf{D}^{-1/2}))_{ij}, \tag{18}$$

where $\mathbf{D}$ is the diagonal degree matrix (Crofts and Higham, 2009). The code to compute communicability in weighted networks is available in the netneurotools python toolbox (https://github.com/netneurolab/netneurotools).

Principal FC gradient

The principal gradient of functional connectivity is thought to reflect the main organizational axis of the brain, ranging from primary sensory and motor regions to transmodal regions (Huntenburg et al., 2018; Margulies et al., 2016). This gradient can be reconstructed using diffusion map embeddding, a nonlinear dimensionality reduction algorithm (Coifman et al., 2005). The algorithm seeks to project a set of embeddings into a lower-dimensional Euclidean space. Briefly, the similarity matrix among a set of points (in our case, the correlation matrix representing functional connectivity) is treated as a graph, and the goal of the procedure is to identify points that are proximal to one another on the graph. In other words, two points are close together if there are many relatively short paths connecting them. A diffusion operator, representing an ergodic Markov chain on the network, is formed by taking the normalized graph Laplacian of the matrix. The new coordinate space is described by the eigenvectors of the diffusion operator. We set the diffusion rate $\alpha = 0.5$. The eigenvalues λ were divided by $1 - \lambda$ to provide noise robustness and eliminate the need for a diffusion time (t) parameter. For each dataset and parcellation, the principal gradient was computed on a consensus functional connectivity matrix computed by averaging the pairwise correlations obtained across individuals and setting the negative values to 0. The procedure was implemented using the mapalign Toolbox (https://github.com/satra/mapalign).

Generative model

A stochastic block model (Holland et al., 1983) was used to generate an artificial network. The edge probability matrix $\mathbf{P}$ was defined to generate an hierarchically modular network of 2000 nodes with a layer of 4 equally-sized communities and another of 2 equally-sized communities:

$$\mathbf{P} = \begin{pmatrix} 0.05 & 0.0125 & 0.005 & 0.005 \\ 0.0125 & 0.05 & 0.005 & 0.005 \\ 0.005 & 0.005 & 0.05 & 0.0125 \\ 0.005 & 0.005 & 0.0125 & 0.05 \end{pmatrix} \tag{19}$$

The specific probabilities were also chosen so that the two-dimensional embedding clearly delineates the four communities of the network. The network was generated using the NetworkX package (Hagberg et al., 2008). The two-dimensional embedding of this network was generated using the ForceAtlas2 algorithm (Jacomy et al., 2014).

Data and code availability

The *Discovery* dataset (Lausanne) is available at https://doi.org/10.5281/zenodo.2872624 and the *Validation* dataset (Human Connectome project) is available at https://www.humanconnectome.org/study/hcp-young-adult. The code used to conduct the analyses presented in this paper is available at https://github.com/netneurolab/bazinet_multiscale.

Declaration of Competing Interests

The authors declare no conflicts of interest.

Credit authorship contribution statement

Vincent Bazinet: Conceptualization, Formal analysis, Investigation, Methodology, Software, Visualization, Writing – original draft, Writing – review & editing. **Reinder Vos de Wael:** Data curation, Resources, Writing – review & editing. **Patric Hagmann:** Data curation, Resources, Writing – review & editing. **Boris C. Bernhardt:** Data curation, Resources, Writing – review & editing. **Bratislav Misic:** Conceptualization, Funding acquisition, Methodology, Project administration, Supervision, Writing – original draft, Writing – review & editing.

Acknowledgments

We thank Laura Suarez, Justine Hansen, Golia Shafiei, Bertha Vazquez-Rodriguez, Ross Markello and Zhen-Qi Liu for insightful comments. VB acknowledges support from the Fonds du Recherche Québec - Nature et Technologies. BM acknowledges support from the Natural Sciences and Engineering Research Council of Canada (NSERC Discovery Grant RGPIN #017-04265), from the Canada Research Chairs Program and from the Canada First Research Excellence Fund, awarded to McGill University for the Healthy Brains for Healthy Lives initiative.

Supplementary material

Supplementary material associated with this article can be found, in the online version, at 10.1016/j.neuroimage.2021.118546

References

Abdelnour, F., Voss, H.U., Raj, A., 2014. Network diffusion accurately models the relationship between structural and functional brain connectivity networks. Neuroimage 90, 335–347.

Alexander-Bloch, A.F., Shou, H., Liu, S., Satterthwaite, T.D., Glahn, D.C., Shinohara, R.T., Vandekar, S.N., Raznahan, A., 2018. On testing for spatial correspondence between maps of human brain structure and function. Neuroimage 178, 540–551.

Avena-Koenigsberger, A., Misic, B., Sporns, O., 2018. Communication dynamics in complex brain networks. Nat Rev Neurosci 19 (1), 17.

Avena-Koenigsberger, A., Yan, X., Kolchinsky, A., van den Heuvel, M., Hagmann, P., Sporns, O., 2019. A spectrum of routing strategies for brain networks. PLoS Comput Biol 15 (3), e1006833.

Bacik, K.A., Schaub, M.T., Beguerisse-Díaz, M., Billeh, Y.N., Barahona, M., 2016. Flow-based network analysis of the caenorhabditis elegans connectome. PLoS Comput Biol 12 (8), e1005055. doi:10.1371/journal.pcbi.1005055.

Bassett, D.S., Meyer-Lindenberg, A., Achard, S., Duke, T., Bullmore, E., 2006. Adaptive reconfiguration of fractal small-world human brain functional networks. Proceedings of the National Academy of Sciences 103 (51), 19518–19523.

Baum, G.L., Cui, Z., Roalf, D.R., Ciric, R., Betzel, R.F., Larsen, B., Cieslak, M., Cook, P.A., Xia, C.H., Moore, T.M., et al., 2020. Development of structure–function coupling in human brain networks during youth. Proceedings of the National Academy of Sciences 117 (1), 771–778.

Bertolero, M.A., Yeo, B.T., Bassett, D.S., D'Esposito, M., 2018. A mechanistic model of connector hubs, modularity and cognition. Nat. Hum. Behav. 2 (10), 765–777.

Bertolero, M.A., Yeo, B.T., D'Esposito, M., 2015. The modular and integrative functional architecture of the human brain. Proceedings of the National Academy of Sciences 112 (49), E6798–E6807.

Bertolero, M.A., Yeo, B.T., D'Esposito, M., 2017. The diverse club. Nat Commun 8 (1), 1–11.

Bettinardi, R.G., Deco, G., Karlaftis, V.M., Van Hartevelt, T.J., Fernandes, H.M., Kourtzi, Z., Kringelbach, M.L., Zamora-López, G., 2017. How structure sculpts function: unveiling the contribution of anatomical connectivity to the brain's spontaneous correlation structure. Chaos 27 (4), 047409.

Betzel, R.F., Bassett, D.S., 2017. Multi-scale brain networks. Neuroimage 160, 73–83. doi:10.1016/j.neuroimage.2016.11.006. http://www.sciencedirect.com/science/article/pii/S1053811916306152

Betzel, R.F., Bassett, D.S., 2018. Specificity and robustness of long-distance connections in weighted, interareal connectomes. Proc Natl Acad Sci USA 115 (21), E4880–E4889. doi:10.1073/pnas.1720186115. https://www.pnas.org/content/115/21/E4880

Betzel, R.F., Byrge, L., He, Y., Goñi, J., Zuo, X.-N., Sporns, O., 2014. Changes in structural and functional connectivity among resting-state networks across the human lifespan. Neuroimage 102, 345–357.

Betzel, R.F., Griffa, A., Avena-Koenigsberger, A., Goñi, J., Thiran, J.-P., Hagmann, P., Sporns, O., 2013. Multi-scale community organization of the human structural connectome and its relationship with resting-state functional connectivity. Network Science 1 (3), 353–373. doi:10.1017/nws.2013.19. https://www.cambridge.org/core/journals/network-science/article/multiscale-community-organization-of-the-human-structural-connectome-and-its-relationship-with-restingstate-functional-connectivity/97B9B699236A2F129684F1D80D1DA220

Betzel, R.F., Griffa, A., Hagmann, P., Mišić, B., 2018. Distance-dependent consensus thresholds for generating group-representative structural brain networks. Net Neurosci 3 (2), 475–496. doi:10.1162/netn_a_00075.

Betzel, R.F., Medaglia, J.D., Bassett, D.S., 2018. Diversity of meso-scale architecture in human and non-human connectomes. Nat Commun 9 (1), 1–14.

Blondel, V.D., Guillaume, J.-L., Lambiotte, R., Lefebvre, E., 2008. Fast unfolding of communities in large networks. J Stat Mech 2008 (10), P10008.

Brin, S., Page, L., 1998. The anatomy of a large-scale hypertextual web search engine. Computer Networks and ISDN Systems 30 (1), 107–117. doi:10.1016/S0169-7552(98)00110-X.

Buckner, R.L., Krienen, F.M., 2013. The evolution of distributed association networks in the human brain. Trends Cogn. Sci. (Regul. Ed.) 17 (12), 648–665.

Buckner, R.L., Sepulcre, J., Talukdar, T., Krienen, F.M., Liu, H., Hedden, T., Andrews-Hanna, J.R., Sperling, R.A., Johnson, K.A., 2009. Cortical hubs revealed by intrinsic functional connectivity: mapping, assessment of stability, and relation to alzheimer's disease. J. Neurosci. 29 (6), 1860–1873.

Bullmore, E., Sporns, O., 2009. Complex brain networks: graph theoretical analysis of structural and functional systems. Nat Rev Neurosci 10 (3), 186–198. doi:10.1038/nrn2575.

Cammoun, L., Gigandet, X., Meskaldji, D., Thiran, J.P., Sporns, O., Do, K.Q., Maeder, P., Meuli, R., Hagmann, P., 2012. Mapping the human connectome at multiple scales with diffusion spectrum MRI. J. Neurosci. Methods 203 (2), 386–397. doi:10.1016/j.jneumeth.2011.09.031. http://www.sciencedirect.com/science/article/pii/S0165027011005991

Chang, A.Y., Biehl, M., Yu, Y., Kanai, R., 2020. Information closure theory of consciousness. Front Psychol 11, 1504.

Coifman, R.R., Lafon, S., Lee, A.B., Maggioni, M., Nadler, B., Warner, F., Zucker, S.W., 2005. Geometric diffusions as a tool for harmonic analysis and structure definition of data: diffusion maps. Proc Natl Acad Sci USA 102 (21), 7426–7431.

Crofts, J.J., Higham, D.J., 2009. A weighted communicability measure applied to complex brain networks. J Roy Soc Interface 6 (33), 411–414.

Daducci, A., Gerhard, S., Griffa, A., Lemkaddem, A., Cammoun, L., Gigandet, X., Meuli, R., Hagmann, P., Thiran, J.-P., 2012. The connectome mapper: an open-source processing pipeline to map connectomes with mri. PLoS ONE 7 (12), e48121.

Demirtaş, M., Burt, J.B., Helmer, M., Ji, J.L., Adkinson, B.D., Glasser, M.F., Van Essen, D.C., Sotiropoulos, S.N., Anticevic, A., Murray, J.D., 2019. Hierarchical heterogeneity across human cortex shapes large-scale neural dynamics. Neuron 101 (6), 1181–1194.

Desikan, R.S., Ségonne, F., Fischl, B., Quinn, B.T., Dickerson, B.C., Blacker, D., Buckner, R.L., Dale, A.M., Maguire, R.P., Hyman, B.T., Albert, M.S., Killiany, R.J., 2006. An automated labeling system for subdividing the human cerebral cortex on MRI scans into gyral based regions of interest. Neuroimage 31 (3), 968–980. doi:10.1016/j.neuroimage.2006.01.021. http://www.sciencedirect.com/science/article/pii/S1053811906000437

Dhollander, T., Raffelt, D., Connelly, A., 2016. Unsupervised 3-tissue response function estimation from single-shell or multi-shell diffusion mr data without a co-registered t1 image. In: ISMRM Workshop on Breaking the Barriers of Diffusion MRI, Vol. 5, p. 5.

von Economo, C.F., Koskinas, G.N., 1925. Die cytoarchitektonik der hirnrinde des erwachsenen menschen. Springer.

von Economo, C.F., Koskinas, G.N., Triarhou, L.C., 2008. Atlas of cytoarchitectonics of the adult human cerebral cortex. Karger Basel.

Estrada, E., Hatano, N., 2008. Communicability in complex networks. Physical Review E 77 (3), 036111.

Faskowitz, J., Yan, X., Zuo, X.-N., Sporns, O., 2018. Weighted stochastic block models of the human connectome across the life span. Sci Rep 8 (1), 1–16.

Fornito, A., Zalesky, A., Bullmore, E., 2016. Fundamentals of brain network analysis. Academic Press, Amsterdam.

Fortunato, S., 2010. Community detection in graphs. Phys Rep 486 (3–5), 75–174.

Glasser, M.F., Sotiropoulos, S.N., Wilson, J.A., Coalson, T.S., Fischl, B., Andersson, J.L., Xu, J., Jbabdi, S., Webster, M., Polimeni, J.R., et al., 2013. The minimal preprocessing pipelines for the human connectome project. Neuroimage 80, 105–124.

Gong, G., He, Y., Concha, L., Lebel, C., Gross, D.W., Evans, A.C., Beaulieu, C., 2009. Mapping anatomical connectivity patterns of human cerebral cortex using in vivo diffusion tensor imaging tractography. Cerebral cortex 19 (3), 524–536.
Goulas, A., Zilles, K., Hilgetag, C.C., 2018. Cortical gradients and laminar projections in mammals. Trends Neurosci 41 (11), 775–788.
Goñi, J., van den Heuvel, M.P., Avena-Koenigsberger, A., de Mendizabal, N.V., Betzel, R.F., Griffa, A., Hagmann, P., Corominas-Murtra, B., Thiran, J.-P., Sporns, O., 2014. Resting-brain functional connectivity predicted by analytic measures of network communication. Proceedings of the National Academy of Sciences 111 (2), 833–838.
Graham, D., Rockmore, D., 2011. The packet switching brain. J Cogn Neurosci 23 (2), 267–276.
Griffa, A., Alemán-Gómez, Y., Hagmann, P., 2019. Structural and functional connectome from 70 young healthy adults. 10.5281/zenodo.2872624. Type: dataset. https://zenodo.org/record/2872624#.XZ5WUnVKifY. 10.5281/zenodo.2872624
Gu, S., Pasqualetti, F., Cieslak, M., Telesford, Q.K., Alfred, B.Y., Kahn, A.E., Medaglia, J.D., Vettel, J.M., Miller, M.B., Grafton, S.T., et al., 2015. Controllability of structural brain networks. Nat Commun 6 (1), 1–10.
Guimera, R., Amaral, L.A.N., 2005. Functional cartography of complex metabolic networks. Nature 433 (7028), 895–900.
Guimera, R., Mossa, S., Turtschi, A., Amaral, L.N., 2005. The worldwide air transportation network: anomalous centrality, community structure, and cities' global roles. Proceedings of the National Academy of Sciences 102 (22), 7794–7799.
Hagberg, A.A., Schult, D.A., Swart, P.J., 2008. Exploring network structure, dynamics, and function using networkx. In: Varoquaux, G., Vaught, T., Millman, J. (Eds.), Proceedings of the 7th Python in Science Conference. Pasadena, CA USA, pp. 11–15.
Hagmann, P., Cammoun, L., Gigandet, X., Meuli, R., Honey, C.J., Wedeen, V.J., Sporns, O., 2008. Mapping the structural core of human cerebral cortex. PLoS Biol 6 (7), e159.
van den Heuvel, M.P., Kahn, R.S., Goñi, J., Sporns, O., 2012. High-cost, high-capacity backbone for global brain communication. Proceedings of the National Academy of Sciences 109 (28), 11372–11377.
van den Heuvel, M.P., Sporns, O., 2013. Network hubs in the human brain. Trends Cogn Sci 17 (12), 683–696. doi:10.1016/j.tics.2013.09.012.
Hilgetag, C.C., Goulas, A., 2020. 'Hierarchy' in the organization of brain networks. Philos Trans R Soc B 375 (1796), 20190319.
Hilgetag, C.C., Kaiser, M., 2004. Clustered organization of cortical connectivity. Neuroinformatics 2 (3), 353–360.
Hilgetag, C.-C., O'Neill, M.A., Young, M.P., 2000. Hierarchical organization of macaque and cat cortical sensory systems explored with a novel network processor. Philos Trans Roy Soc B 355 (1393), 71–89.
Holland, P.W., Laskey, K.B., Leinhardt, S., 1983. Stochastic blockmodels: first steps. Soc Networks 5 (2), 109–137.
Huntenburg, J.M., Bazin, P.-L., Margulies, D.S., 2018. Large-scale gradients in human cortical organization. Trends Cogn. Sci. (Regul. Ed.) 22 (1), 21–31.
Ito, T., Hearne, L.J., Cole, M.W., 2020. A cortical hierarchy of localized and distributed processes revealed via dissociation of task activations, connectivity changes, and intrinsic timescales. Neuroimage. –
Jacomy, M., Venturini, T., Heymann, S., Bastian, M., 2014. Forceatlas2, a continuous graph layout algorithm for handy network visualization designed for the gephi software. PLoS ONE 9 (6).
Jeurissen, B., Tournier, J.-D., Dhollander, T., Connelly, A., Sijbers, J., 2014. Multi-tissue constrained spherical deconvolution for improved analysis of multi-shell diffusion mri data. Neuroimage 103, 411–426.
Kaiser, M., Hilgetag, C.C., Kötter, R., 2010. Hierarchy and dynamics of neural networks. Front Neuroinformatics 4, 112.
Klein, B., Hoel, E., 2020. The emergence of informative higher scales in complex networks. Complexity 2020.
Lancichinetti, A., Fortunato, S., 2012. Consensus clustering in complex networks. Sci Rep 2, 336.
Maier-Hein, K.H., Neher, P.F., Houde, J.-C., Côté, M.-A., Garyfallidis, E., Zhong, J., Chamberland, M., Yeh, F.-C., Lin, Y.-C., Ji, Q., et al., 2017. The challenge of mapping the human connectome based on diffusion tractography. Nat Commun 8 (1), 1–13.
Margulies, D.S., Ghosh, S.S., Goulas, A., Falkiewicz, M., Huntenburg, J.M., Langs, G., Bezgin, G., Eickhoff, S.B., Castellanos, F.X., Petrides, M., Jeffries, E., Smallwood, J., 2016. Situating the default-mode network along a principal gradient of macroscale cortical organization. Proc Natl Acad Sci USA 113 (44), 12574–12579.
Markello, R.D., Misic, B., 2021. Comparing spatial null models for brain maps. Neuroimage 236, 118052.
Mars, R.B., Passingham, R.E., Jbabdi, S., 2018. Connectivity fingerprints: from areal descriptions to abstract spaces. Trends Cogn Sci 22 (11), 1026–1037.
Masuda, N., Porter, M.A., Lambiotte, R., 2017. Random walks and diffusion on networks. Phys Rep 716, 1–58.
Mišić, B., Betzel, R.F., Griffa, A., De Reus, M.A., He, Y., Zuo, X.-N., Van Den Heuvel, M.P., Hagmann, P., Sporns, O., Zatorre, R.J., 2018. Network-based asymmetry of the human auditory system. Cereb Cortex 28 (7), 2655–2664.
Mišić, B., Betzel, R.F., Nematzadeh, A., Goni, J., Griffa, A., Hagmann, P., Flammini, A., Ahn, Y.-Y., Sporns, O., 2015. Cooperative and competitive spreading dynamics on the human connectome. Neuron 86 (6), 1518–1529.
Oligschläger, S., Huntenburg, J.M., Golchert, J., Lauckner, M.E., Bonnen, T., Margulies, D.S., 2017. Gradients of connectivity distance are anchored in primary cortex. Brain Struct Funct 222 (5), 2173–2182.
Oligschläger, S., Xu, T., Baczkowski, B.M., Falkiewicz, M., Falchier, A., Linn, G., Margulies, D.S., 2019. Gradients of connectivity distance in the cerebral cortex of the macaque monkey. Brain Struct Funct 224 (2), 925–935.
Onnela, J.-P., Saramäki, J., Kertész, J., Kaski, K., 2005. Intensity and coherence of motifs in weighted complex networks. Physical Review E 71 (6), 065103.
Paquola, C., De Wael, R.V., Wagstyl, K., Bethlehem, R.A., Hong, S.-J., Seidlitz, J., Bullmore, E.T., Evans, A.C., Misic, B., Margulies, D.S., et al., 2019. Microstructural and functional gradients are increasingly dissociated in transmodal cortices. PLoS Biol. 17 (5), e3000284.
Park, B.-y., de Wael, R.V., Paquola, C., Larivière, S., Benkarim, O., Royer, J., Tavakol, S., Cruces, R.R., Li, Q., Valk, S.L., et al., 2021. Signal diffusion along connectome gradients and inter-hub routing differentially contribute to dynamic human brain function. Neuroimage 117429.
Passingham, R.E., Stephan, K.E., Kötter, R., 2002. The anatomical basis of functional localization in the cortex. Nat Rev Neurosci 3 (8), 606–616.
Pavlovic, D.M., Vértes, P.E., Bullmore, E.T., Schafer, W.R., Nichols, T.E., 2014. Stochastic blockmodeling of the modules and core of the caenorhabditis elegans connectome. PLoS ONE 9 (7), e97584.
Pedersen, M., Omidvarnia, A., Shine, J.M., Jackson, G.D., Zalesky, A., 2020. Reducing the influence of intramodular connectivity in participation coefficient. Net Neurosci 4 (2), 416–431.
Poldrack, R.A., Kittur, A., Kalar, D., Miller, E., Seppa, C., Gil, Y., Parker, D.S., Sabb, F.W., Bilder, R.M., 2011. The cognitive atlas: toward a knowledge foundation for cognitive neuroscience. Front Neuroinform 5, 17.
Power, J.D., Barnes, K.A., Snyder, A.Z., Schlaggar, B.L., Petersen, S.E., 2012. Spurious but systematic correlations in functional connectivity mri networks arise from subject motion. Neuroimage 59 (3), 2142–2154.
Power, J.D., Schlaggar, B.L., Lessov-Schlaggar, C.N., Petersen, S.E., 2013. Evidence for hubs in human functional brain networks. Neuron 79 (4), 798–813.
Preti, M.G., Van De Ville, D., 2019. Decoupling of brain function from structure reveals regional behavioral specialization in humans. Nat Commun 10 (1), 1–7.
Rosvall, M., Bergstrom, C.T., 2008. Maps of random walks on complex networks reveal community structure. Proceedings of the National Academy of Sciences 105 (4), 1118–1123.
Rubinov, M., Sporns, O., 2010. Complex network measures of brain connectivity: uses and interpretations. Neuroimage 52 (3), 1059–1069.
Schaefer, A., Kong, R., Gordon, E.M., Laumann, T.O., Zuo, X.-N., Holmes, A.J., Eickhoff, S.B., Yeo, B.T.T., 2018. Local-global parcellation of the human cerebral cortex from intrinsic functional connectivity MRI. Cereb Cortex 28 (9), 3095–3114. doi:10.1093/cercor/bhx179. https://academic.oup.com/cercor/article/28/9/3095/3978804
Schaub, M.T., Delvenne, J.-C., Lambiotte, R., Barahona, M., 2019. Multiscale dynamical embeddings of complex networks. Physical Review E 99 (6), 062308.
Sepulcre, J., Liu, H., Talukdar, T., Martincorena, I., Yeo, B.T., Buckner, R.L., 2010. The organization of local and distant functional connectivity in the human brain. PLoS Comput Biol 6 (6), e1000808.
Smith, R.E., Tournier, J.-D., Calamante, F., Connelly, A., 2015. Sift2: enabling dense quantitative assessment of brain white matter connectivity using streamlines tractography. Neuroimage 119, 338–351.
Sporns, O., 2013. Network attributes for segregation and integration in the human brain. Curr. Opin. Neurobiol. 23 (2), 162–171.
Sporns, O., Honey, C.J., Kötter, R., 2007. Identification and classification of hubs in brain networks. PLOSONE 2 (10), e1049. doi:10.1371/journal.pone.0001049.
Suárez, L.E., Markello, R.D., Betzel, R.F., Misic, B., 2020. Linking structure and function in macroscale brain networks. Trends Cogn. Sci. (Regul. Ed.) 24 (4), 302–315. doi:10.1016/j.tics.2020.01.008.
Thomas, C., Frank, Q.Y., Irfanoglu, M.O., Modi, P., Saleem, K.S., Leopold, D.A., Pierpaoli, C., 2014. Anatomical accuracy of brain connections derived from diffusion mri tractography is inherently limited. Proceedings of the National Academy of Sciences 111 (46), 16574–16579.
Tononi, G., Edelman, G.M., Sporns, O., 1998. Complexity and coherency: integrating information in the brain. Trends Cogn. Sci. (Regul. Ed.) 2 (12), 474–484.
Tournier, J.-D., Smith, R., Raffelt, D., Tabbara, R., Dhollander, T., Pietsch, M., Christiaens, D., Jeurissen, B., Yeh, C.-H., Connelly, A., 2019. Mrtrix3: a fast, flexible and open software framework for medical image processing and visualisation. Neuroimage 202, 116137.
Traud, A.L., Kelsic, E.D., Mucha, P.J., Porter, M.A., 2011. Comparing community structure to characteristics in online collegiate social networks. SIAM Rev. 53 (3), 526–543.
Trusina, A., Rosvall, M., Sneppen, K., 2005. Communication boundaries in networks. Phys. Rev. Lett. 94 (23), 238701.
Van Den Heuvel, M.P., Sporns, O., 2011. Rich-club organization of the human connectome. J. Neurosci. 31 (44), 15775–15786.
Van Essen, D.C., Smith, S.M., Barch, D.M., Behrens, T.E.J., Yacoub, E., Ugurbil, K., 2013. The WU-minn human connectome project: an overview. Neuroimage 80, 62–79. doi:10.1016/j.neuroimage.2013.05.041. http://www.sciencedirect.com/science/article/pii/S1053811913005351
Váša, F., Seidlitz, J., Romero-Garcia, R., Whitaker, K.J., Rosenthal, G., Vértes, P.E., Shinn, M., Alexander-Bloch, A., Fonagy, P., Dolan, R.J., et al., 2018. Adolescent tuning of association cortex in human structural brain networks. Cerebral Cortex 28 (1), 281–294.
Vázquez-Rodríguez, B., Suárez, L.E., Markello, R.D., Shafiei, G., Paquola, C., Hagmann, P., Van Den Heuvel, M.P., Bernhardt, B.C., Spreng, R.N., Misic, B., 2019. Gradients of structure–function tethering across neocortex. Proceedings of the National Academy of Sciences 116 (42), 21219–21227.
Vértes, P.E., Rittman, T., Whitaker, K.J., Romero-Garcia, R., Váša, F., Kitzbichler, M.G., Wagstyl, K., Fonagy, P., Dolan, R.J., Jones, P.B., et al., 2016. Gene transcription profiles associated with inter-modular hubs and connection distance in human functional magnetic resonance imaging networks. Phil Trans R Soc B 371 (1705), 20150362.
Wang, P., Kong, R., Kong, X., Liégeois, R., Orban, C., Deco, G., Van Den Heuvel, M.P., Yeo, B.T., 2019. Inversion of a large-scale circuit model reveals a cortical hierarchy in the dynamic resting human brain. Sci Adv 5 (1), eaat7854.

Watts, D.J., Strogatz, S.H., 1998. Collective dynamics of 'small-world' networks. Nature 393 (6684), 440–442. doi:10.1038/30918.

Yarkoni, T., Poldrack, R.A., Nichols, T.E., Van Essen, D.C., Wager, T.D., 2011. Large-scale automated synthesis of human functional neuroimaging data. Nat. Methods 8 (8), 665–670.

Yeo, B.T.T., Krienen, F.M., Sepulcre, J., Sabuncu, M.R., Lashkari, D., Hollinshead, M., Roffman, J.L., Smoller, J.W., Zöllei, L., Polimeni, J.R., Fischl, B., Liu, H., Buckner, R.L., 2011. The organization of the human cerebral cortex estimated by intrinsic functional connectivity. J. Neurophysiol. 106 (3), 1125–1165. doi:10.1152/jn.00338.2011.

Zalesky, A., Fornito, A., Harding, I.H., Cocchi, L., Yücel, M., Pantelis, C., Bullmore, E.T., 2010. Whole-brain anatomical networks: does the choice of nodes matter? Neuroimage 50 (3), 970–983.

Zamora-López, G., Zhou, C., Kurths, J., 2009. Graph analysis of cortical networks reveals complex anatomical communication substrate. Chaos 19 (1), 015117.

Zamora-López, G., Zhou, C., Kurths, J., 2010. Cortical hubs form a module for multisensory integration on top of the hierarchy of cortical networks. Front Neuroinform 4, 1.

Zhou, C., Zemanová, L., Zamora, G., Hilgetag, C.C., Kurths, J., 2006. Hierarchical organization unveiled by functional connectivity in complex brain networks. Phys Rev Lett 97 (23), 238103.

Zuo, X.-N., Ehmke, R., Mennes, M., Imperati, D., Castellanos, F.X., Sporns, O., Milham, M.P., 2012. Network centrality in the human functional connectome. Cereb Cortex 22 (8), 1862–1875. doi:10.1093/cercor/bhr269. https://academic.oup.com/cercor/article/22/8/1862/321860